Application of System Equivalent Model Mixing (SEMM) to model the structural dynamic properties of a complex vehicle component using numerical and experimental data

Pasma, E.; Klaassen, S.; Nieuwenhuijse, L.; Van Der Seijs, M.; Lennström, D.

Publication date
2018

Published in
Proceedings ofthe 28th International Conference on Noise and Vibration Engineering (ISMA 2018) and the 7th International Conference on Uncertainty in Structural Dynamics (USD 2018)

Citation (APA)
Pasma, E., Klaassen, S., Nieuwenhuijse, L., Van Der Seijs, M., & Lennström, D. (2018). Application of System Equivalent Model Mixing (SEMM) to model the structural dynamic properties of a complex vehicle component using numerical and experimental data. In D. Moens, W. Desmet, B. Pluymers, & W. Rottiers (Eds.), *Proceedings ofthe 28th International Conference on Noise and Vibration Engineering (ISMA 2018) and the 7th International Conference on Uncertainty in Structural Dynamics (USD 2018)* (pp. 4037-4047). KU Leuven.

Important note
To cite this publication, please use the final published version (if applicable).
Please check the document version above.

Application of System Equivalent Model Mixing (SEMM) to model the structural dynamic properties of a complex vehicle component using numerical and experimental data

E. Pasma[1], **S. Klaassen**[2], **L. Nieuwenhuijse**[1,3], **M. van der Seijs**[1,3], **D. Lennström**[4]
[1] VIBES.technology
Molengraaffsingel 14, 2629 JD, Delft, The Netherlands,
e-mail: **epasma@vibestechnology.com**

[2] Technische Universität München, Faculty of Mechanical Engineering, Institute of Applied Mechanics, Boltzmannstr. 15, 85748 Garching, Germany

[3] Delft University of Technology, Department of Precision and Microsystems Engineering
Mekelweg 2, 2628CD, Delft, The Netherlands

[4] VOLVO CAR GROUP,
91610, Torslanda PV32, SE-405 31, Göteborg, Sweden

Abstract
A popular strategy in structural dynamic modelling is breaking the structure down into separable, manageable substructures. One can choose the most efficient way of modelling the substructures, before synthesizing the full system model. System Equivalent Model Mixing (SEMM) is a new method that allows mixing of frequency-based models, either of numerical or experimental nature, to form a hybrid structural dynamic model. The method expands measured data onto a numerical mode manifold using Lagrange-Multiplier Frequency Based Substructuring (LM-FBS). Hence, SEMM combines the DoF-space of the numerical model with the dynamic properties of the measured substructure. In this paper, SEMM is applied to a complex vehicle component. Frequency Response Function (FRF) measurements on the component are used to enrich the uncalibrated Finite Element Model of the component. The resulting hybrid model comprises interfaces in six degrees of freedom, which is required for the connectivity to neighboring structures in the FBS framework.

Introduction

Engineers in the automotive industry are faced with numerous challenges. First of all, the demand for shorter product development cycles and fewer physical prototypes is rising, whilst the number of products (or variants) is growing. Moreover, the complexity, functionality and attribute demands (such as NVH, emissions, weight, durability, safety, handling) are increasing.

One of the ways to keep up with these trends, is adopting a modular way of working. For the particular field of sound and vibration engineering, Dynamic Substructuring (DS) is an often-chosen approach. This technique allows the combination of component models coming from different sources (test or numerical), in order to simulate the sound and vibration performance of the full product. Using DS, optimisation of the individual components is possible, while simultaneously respecting the NVH signature of the full vehicle.

Secondly, automotive electrification is becoming more and more prevalent. In traditional vehicles, the internal combustion engine masks the bulk of NVH-problems. On the other hand – in electric vehicles – tonal components become more dominant at higher frequencies (> 1 kHz) [1]. Full (virtual) vehicle simulations

with (deterministic) numerical approaches (e.g. Finite Element Analysis) are pushed towards their limits. Due to this increasing frequency band and desired accuracy, a trend towards test-based modelling strategies is unavoidable.

One recently developed and promising method that fits both in the modular modelling approach and is able to capture complex dynamic behaviour of a structure, is System Equivalent Model Mixing (SEMM). This method allows mixing of frequency-based models, either of numerical or experimental nature, to form a hybrid structural dynamic model. The method expands measured data onto a numerical mode manifold, using theory derived from Lagrange-Multiplier Frequency Based Substructuring (LM-FBS). Therefore, SEMM exploits the best of both domains, by combining the DoF-space of the numerical model with the dynamic properties of the measured substructure.

Paper goal & outline

The main goal of this paper is to show how SEMM is used to model the structural dynamics of the subframe of a vehicle. This subframe hosts an electric drive unit (EDU) which is used for the propulsion of a hybrid vehicle. The second goal is to show how this model is used in the experimental Dynamic Substructuring (DS) Framework. The components considered in this DS application are depicted in figure 1.

The first part of the paper covers the theory on LM-FBS, SEMM and the Virtual Point Transformation. In the second part, the subframe is modelled according to the SEMM method, whereafter it is coupled with LM-FBS to four rubber decoupling elements and a test-based model of the EDU. The test-based modelling of the EDU and the characterisation of the rubber decoupling elements is beyond the scope of this paper.

Figure 1: On the left, a picture of the SEMM measurement set-up. On the right, an overview of the FBS case. The red arrow indicates the force excitation, the blue circle the location of the validation sensor.

1 Theory

The contents of this section is divided into three parts. The first section will briefly explain the dual solution of experimental dynamic substructuring in the frequency domain along with the definition and inclusion of weak interfaces. The second part covers the theory of the SEMM-method, tailored to the envisioned application. Last, a short recap on the virtual point transformation is provided.

1.1 Lagrange Multiplier Frequency Based Substructuring

DS is applied in this work with the Lagrange Multiplier Frequency Based Substructuring (LM-FBS) method [2]. As the name implies, LM-FBS is applied in the frequency domain and its main strength lies in the fact

that it works in the admittance space; this allows for direct implementation of experimental measurement results. This makes it the preferred DS method when working with experimental models.

The equation of motion to couple two arbitrary systems with LM-FBS is as follows:

$$\mathbf{u} = \mathbf{Y}\left(\mathbf{f} + \mathbf{g}\right), \quad \text{with} \quad \mathbf{Y} = \begin{bmatrix} \mathbf{Y}^{\mathrm{A}} & \\ & \mathbf{Y}^{\mathrm{B}} \end{bmatrix}, \quad \mathbf{f} = \begin{bmatrix} \mathbf{f}^{\mathrm{A}} \\ \mathbf{f}^{\mathrm{B}} \end{bmatrix}, \quad \mathbf{g} = \begin{bmatrix} \mathbf{g}^{\mathrm{A}} \\ \mathbf{g}^{\mathrm{B}} \end{bmatrix} \tag{1}$$

Where $\mathbf{u}$ is the vector of dynamic displacements, $\mathbf{Y}$ is an admittance FRF matrix, $\mathbf{f}$ is a vector of applied forces and $\mathbf{g}$ is a vector of interface forces. The displacement and force vectors can contain rotations and moments, respectively. Equation (1) is subject to two sets of constraints: the compatibility and equilibrium conditions. First, the compatibility condition states:

$$\mathbf{u}_b^{\mathrm{A}} - \mathbf{u}_b^{\mathrm{B}} = \mathbf{0} \quad \rightarrow \quad \mathbf{B}\mathbf{u} = \mathbf{0} \tag{2}$$

Where $\mathbf{B}$ is a signed Boolean matrix explicitly stating a relation between the boundary DoF. It has the form:

$$\mathbf{B} = \begin{bmatrix} \mathbf{0} & \mathbf{I} & \mathbf{0} & -\mathbf{I} \end{bmatrix} \tag{3}$$

Where the columns of $\mathbf{B}$ refer to the elements in $\mathbf{u} = \begin{bmatrix} \mathbf{u}_i^{\mathrm{A}} & \mathbf{u}_b^{\mathrm{A}} & \mathbf{u}_i^{\mathrm{B}} & \mathbf{u}_b^{\mathrm{B}} \end{bmatrix}^T$ and the rows refer to number of compatibility equations. The equilibrium condition enforces force equilibrium on the boundary:

$$\mathbf{g}_b^{\mathrm{A}} = \mathbf{g}_b^{\mathrm{B}} = \boldsymbol{\lambda} \quad \rightarrow \quad \mathbf{B}^T\boldsymbol{\lambda} = -\mathbf{g} \tag{4}$$

Where the same coupling matrix in definition (3) is used. Equation (1) is solved by inserting the compatibility equation (2) and the equilibrium equation (4) and solving for $\boldsymbol{\lambda}$. Equation (5) is then re-applied into equation (1) to find the coupled dynamics.

$$\boldsymbol{\lambda} = \left(\mathbf{B}\mathbf{Y}\mathbf{B}^T\right)^{-1}\mathbf{B}\mathbf{Y}\mathbf{f} \tag{5}$$

$$\mathbf{u} = \mathbf{Y}\mathbf{f} - \mathbf{Y}\mathbf{B}^T\left(\mathbf{B}\mathbf{Y}\mathbf{B}^T\right)^{-1}\mathbf{B}\mathbf{Y}\mathbf{f} \tag{6}$$

The coupled model thus becomes:

$$\mathbf{Y}^{\mathrm{AB}} = \mathbf{Y} - \mathbf{Y}\mathbf{B}^T\left(\mathbf{B}\mathbf{Y}\mathbf{B}^T\right)^{-1}\mathbf{B}\mathbf{Y} \tag{7}$$

1.1.1 Interface weakening in LM-FBS

Equation (2) assumes a rigid connection since it requires a 1-to-1 relation. Yet the connection can also be weakened by allowing a gap to exist in the boundary displacements [3]. This means that a gap is allowed in the compatibility, i.e. equation (2) is reformulated:

$$\mathbf{B}\mathbf{u} = \boldsymbol{\Delta}\mathbf{u}_b \tag{8}$$

The gap $\boldsymbol{\Delta}\mathbf{u}_b$ is maintained by joint stiffness $\mathbf{K}^{\mathrm{J}}$ and damping $\mathbf{C}^{\mathrm{J}}$ when enforced by the boundary forces described by $\boldsymbol{\lambda}$. Note that sithese terms only denote the connection stiffness and damping between the interfaces of both sides. Mathematically, they represent the off-diagonal terms of the joint.

$$\mathbf{C}^{\mathrm{J}}\boldsymbol{\Delta}\dot{\mathbf{u}}_b(t) + \mathbf{K}^{\mathrm{J}}\boldsymbol{\Delta}\mathbf{u}_b(t) = \boldsymbol{\lambda}(t) \quad \rightarrow \quad \mathbf{Z}^{\mathrm{J}}\boldsymbol{\Delta}\mathbf{u}_b(\omega) = \boldsymbol{\lambda}(\omega) \quad \rightarrow \quad \boldsymbol{\Delta}\mathbf{u}_b(\omega) = \mathbf{Y}^{\mathrm{J}}\boldsymbol{\lambda}(\omega) \tag{9}$$

Note that in the weakening assumption no mass terms exist in the joint; the inertial forces from a mass contribution would mean equation (4) no longer holds.

The weakened LM-FBS can then be derived by first deriving the boundary forces $\boldsymbol{\lambda}$ and then solving the constrained equation of motion (1) like before (for the full derivation, see [3]):

$$\boldsymbol{\lambda} = \left(\mathbf{B}\mathbf{Y}\mathbf{B}^T + \mathbf{Y}^{\mathrm{J}}\right)^{-1}\mathbf{B}\mathbf{Y}\mathbf{f} \tag{10}$$

$$\mathbf{Y}^{\mathrm{AJB}} = \mathbf{Y} - \mathbf{Y}\mathbf{B}^T\left(\mathbf{B}\mathbf{Y}\mathbf{B}^T + \mathbf{Y}^{\mathrm{J}}\right)^{-1}\mathbf{B}\mathbf{Y} \tag{11}$$

Where the addition of the superscript $(\bullet)^{\mathrm{J}}$ to $\mathbf{Y}^{\mathrm{AJB}}$ in equation (11) indicates that the joint dynamics have been included in the formulation.

1.2 System Equivalent Model Mixing

For SEMM, a few "building blocks" are needed. First, the **parent** models $\mathbf{Y}^{\text{par}}$ are the models of the system which will be mixed. In the proposed case they are the numerical FE-model and the experimental measurements of the component. The FE-model, which could potentially contain any desired DoF, acts as the manifold composed of the equivalent-experimental-DoFs and the expansion DoF-set. The experimental measurements are deemed a more accurate representation of the complex component's physics and will be considered the more trusted information source throughout the frequency range.

Next, the overlay and removed model are defined. The **overlay** model $\mathbf{Y}^{\text{ov}}$ is the model which will determine the dynamic properties of the hybrid model and is therefore a trusted (sub)set of the **experimental** model. The **removed** model $\mathbf{Y}^{\text{rem}}$ is a (sub)set of the **numerical** manifold which contains the DoFs overlapping with the overlay model.

Translating this to classic DS notations, the expanded DoF are internal DoF unique to the numerical parent model which will be denoted by $\mathbf{u}_i$; following this conjecture the shared DoFs are boundary DoFs which are denoted by $\mathbf{u}_b$. Therefore the previously introduced building blocks become:

$$\mathbf{Y}^{\text{par, Num.}} = \mathbf{Y}^{\text{rem}} = \begin{bmatrix} \mathbf{Y}_{ii} & \mathbf{Y}_{ib} \\ \mathbf{Y}_{bi} & \mathbf{Y}_{bb} \end{bmatrix}^{\text{Num.}}, \qquad \mathbf{Y}^{\text{par, Exp.}} = \mathbf{Y}^{\text{ov}} = \begin{bmatrix} \mathbf{Y}_{bb} \end{bmatrix}^{\text{Exp.}} \tag{12}$$

Generally the removed model must contain, but is not limited to the boundary DoF. In the case of a full system decoupling, as applied in this work, the removed model is equal to the numerical parent model; more information can be found in [4]. Likewise, the overlay model and experimental parent model are identical; assuming the entirety of the experimental measurements DoF is deemed a trusted set. In light of this, since the experimental parent model is no longer needed, the parent model will now refer to the numerical parent model throughout this work:

$$\mathbf{Y}^{\text{par}} = \mathbf{Y}^{\text{par, Num.}} = \mathbf{Y}^{\text{rem}}, \qquad \mathbf{Y}^{\text{ov}} = \mathbf{Y}^{\text{Exp.}} \tag{13}$$

SEMM is based on DS on an abstract level; the problem is solved by solving (1) for the SEMM abstract system:

$$\mathbf{u} = \mathbf{Y}\left(\mathbf{f} - \mathbf{g}\right), \quad \text{with} \quad \mathbf{Y} = \begin{bmatrix} \mathbf{Y}^{\text{par}} & & \\ & -\mathbf{Y}^{\text{rem}} & \\ & & \mathbf{Y}^{\text{ov}} \end{bmatrix}, \quad \mathbf{f} = \begin{bmatrix} \mathbf{f}^{\text{par}} \\ \mathbf{f}^{\text{rem}} \\ \mathbf{f}^{\text{ov}} \end{bmatrix} = \begin{matrix} \\ \mathbf{0} \\ \mathbf{0} \end{matrix}, \quad \mathbf{g} = \begin{bmatrix} \mathbf{g}^{\text{par}} \\ \mathbf{g}^{\text{rem}} \\ \mathbf{g}^{\text{ov}} \end{bmatrix} \tag{14}$$

Note that the external forces are only applied on the parent model. There is no physical force exerted on the removed and overlay model as they are merely used to apply boundary conditions on the parent model to update its dynamics.

To solve (14) the compatibility and equilibrium constraints are applied as in LM-FBS. Compatibility requires:

$$\mathbf{u}^{\text{par}} - \mathbf{u}^{\text{rem}} = \mathbf{0} \tag{15a}$$

$$\mathbf{u}_b^{\text{rem}} - \mathbf{u}^{\text{ov}} = \mathbf{0} \tag{15b}$$

Note that the relationship is explicit between the parent and removed model, and then between the removed and overlay model. The removed model essentially acts as a conduit, yet note that implicitly a relationship between the overlay model and parent model also exists. Equation (15) can be rewritten in matrix form as in equation (2) with the signed Boolean matrix defined as (using $\mathbf{u} = \begin{bmatrix} \mathbf{u}_i^{\text{par}} & \mathbf{u}_b^{\text{par}} & \mathbf{u}_i^{\text{rem}} & \mathbf{u}_b^{\text{rem}} & \mathbf{u}_b^{\text{ov}} \end{bmatrix}^T$):

$$\mathbf{B} = \begin{bmatrix} \mathbf{I} & \mathbf{0} & -\mathbf{I} & \mathbf{0} & \mathbf{0} \\ \mathbf{0} & \mathbf{I} & \mathbf{0} & -\mathbf{I} & \mathbf{0} \\ \mathbf{0} & \mathbf{0} & \mathbf{0} & \mathbf{I} & -\mathbf{I} \end{bmatrix} \tag{16}$$

This matrix is also used in the equilibrium condition as in equation (4). In this case the equilibrium enforces the following:

$$\mathbf{g}_i^{\text{par}} + \mathbf{g}_i^{\text{rem}} = \mathbf{0} \tag{17a}$$

$$\mathbf{g}_b^{\text{par}} + \mathbf{g}_b^{\text{rem}} + \mathbf{g}^{\text{ov}} = \mathbf{0} \tag{17b}$$

It is apparent that the problem follows the LM-FBS notation as described before. The SEMM problem can therefore be solved with equation (7). It is shown that from this solution the single line of SEMM can be obtained. The derivation is omitted in this paper, the interested reader is recommended to read [4]:

$$\mathbf{Y}^{\text{SEMM}} = \mathbf{Y}^{\text{par}} - \mathbf{Y}^{\text{par}} \left(\mathbf{Y}_{bg}^{\text{rem}}\right)^{+} \left(\mathbf{Y}_{bb}^{\text{rem}} - \mathbf{Y}_{bb}^{\text{ov}}\right) \left(\mathbf{Y}_{gb}^{\text{rem}}\right)^{+} \mathbf{Y}^{\text{par}} \tag{18}$$

Where the subscript $(\bullet)_g$ denotes the global set of DoF, i.e. $g = [i; b]$

1.3 Virtual Point Transformation

The compatibility and equilibrium conditions require that substructures have collocated DoFs: the boundary DoFs. Acquiring collocated DoF in experiments is not trivial since it is often not possible to measure at connection locations.

In order to still create these collocated DoF, the virtual point transformation can be used to create virtual nodes with DoF shared by both sides of a structure. The virtual node is created by rigid transformation of a set of DoF to a 6-DoF (three translations and three rotations) point in space, preferably at the location of the contact [5].

$$\mathbf{u} = \mathbf{R}_{\text{u}}\mathbf{q}, \qquad \mathbf{m} = \mathbf{R}_{\text{f}}^{T}\mathbf{f} \tag{19}$$

Where $\mathbf{R}_{\text{u}}$ and $\mathbf{R}_{\text{f}}$ are rigid transformation matrices transforming from the virtual displacements and forces $\mathbf{q}, \mathbf{m}$ to the measured displacements and forces $\mathbf{u}, \mathbf{f}$. In order to create a full-rank 6-DoF virtual node, at least 6 linear independent functions are needed, i.e. 6 or more displacement and force DoF are required in the input vectors $\mathbf{u}, \mathbf{f}$. Next, $\mathbf{R}_{\text{u}}$ and $\mathbf{R}_{\text{f}}$ are (least-square) inverted and used as the transformation matrices to the virtual locations such that the VP transformed model becomes:

$$\mathbf{Y}^{\text{VP}} = \left(\mathbf{R}_{\text{u}}{}^{T}\mathbf{R}_{\text{u}}\right)^{-1} \mathbf{R}_{\text{u}}\mathbf{Y}\mathbf{R}_{\text{f}} \left(\mathbf{R}_{\text{f}}{}^{T}\mathbf{R}_{\text{f}}\right)^{-1} = \left(\mathbf{R}_{\text{u}}\right)^{+} \mathbf{Y} \left(\mathbf{R}_{\text{f}}^{T}\right)^{+} \tag{20}$$

Where $\mathbf{Y}^{\text{VP}}$ is the virtual point transformed FRF matrix.

Note that the rigid transformation inherently means that a rigid interface assumption is made. If flexibility exists between the virtual node and the input DoF the rigid transformation will no longer adequately describe the correct dynamics [6]. It is therefore important to choose input DoF close to the connection point, such that the rigid interface assumption holds.

2 Application

In this section the test case is presented. The ultimate goal is to obtain a full system FRF model comprising models of the EDU, the rubber decoupling mounts and the subframe through the Frequency Based Substructuring coupling procedure. This model should provide the transfer functions such that the vibration transmission from the EDU to a point of interest can be studied. In NVH engineering, the structure-borne noise at the driver's ears originating from the source is of great concern/interest. To achieve this goal, first accurate individual subsystem FRF models have to be obtained separately, with correct coupling interfaces. This is achieved by building 6 Cartesian translational and rotational DoFs by using the virtual point transformation (section 1.3). This is a prerequisite for successful FBS in the 0 - 2 kHz frequency range of interest [7]. In the following, the modelling techniques for the sub-components are listed:

- *Electric drive unit*: A test-based FRF model by application of the virtual point transformation [5] on the four coupling points of the motor;
- *Rubber decoupling mounts*: The transfer stiffnesses of the four rubber decoupling elements are obtained by an in-situ characterisation approach [8];
- *Subframe*: An FRF model is obtained through SEMM, see section 1.2.

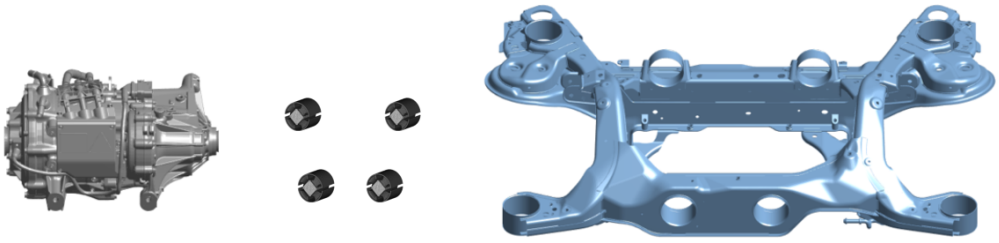

Figure 2: Overview the components in the test case. The EDU connects through four decoupling mounts to the subframe. From left to right: the electric drive unit, the rubber mounts and the subframe.

In this paper, only the SEMM application on the subframe is shown. Using SEMM for the subframe is driven by basically two factors. Firstly, the subframe is a complex system (high modal density), for which the mode shapes can be obtained easily, but the exact eigen-frequencies and damping factors are more challenging. Secondly, there is a limit on the available measurement equipment (for e.g. a full test based model, see section 1.3). In section 2.1.1 a more elaborate motivation for using SEMM is discussed.

2.1 SEMM Application

2.1.1 Motivation to use SEMM

The subframe is a relatively complex DS case as it includes components with up to eight connecting interfaces. Using the virtual point method on each interface would therefore require either up to 24 different sensors, or exhausting roving sensor measurements, in order to create enough linearly independent functions in the FRF-matrix.

In such cases, expansion techniques become an interesting alternative. A few methods exist, all of which would require some notion of an expansion matrix; which, in turn, is mostly extracted out of numerical data. Even fewer are the methods that work well with experimental FRF-data: SEREP, its expansion VIKING and SEMM are the most notable examples.

In order to create per-point linear independent FRF (As required for the virtual points) there are some restrictions: namely that for each point a minimum of 6 linearly independent functions exist in the FRF-subset used in virtual point minimization, i.e. the rank of the said FRF matrix is ≥ 6. Additionally, in order to observe the dynamics of the 8×6 point connections, a minimum of $8 \times 6 = 48$ linearly independent functions should exist in the expanded model. For SEREP, this would mean that a minimum of 48 sensor channels must exist, even more to obtain clean filtered results [9]. VIKING can include numerical data in the expansion and therefore would not require as many sensors per se [10]. It would then however, require a modal fitting of the experimental data; with the modal density of the subframe's FRF, this is an ardous process to this date. SEMM includes the numerical data from the numerical parent model implicitly, consequently the hybrid model's rank is equal to the numerical model's rank (generally full rank). In conclusion, the hybrid model's expanded DoFs can not only be used in the virtual point creation, but also in the DS coupling.

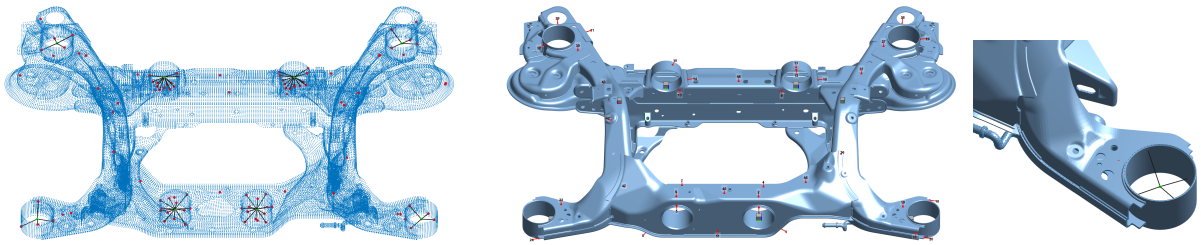

Figure 3: The parent, overlay and resulting SEMM model.

2.1.2 Practical considerations

For the successful application of SEMM, one has to consider some practicalities concerning the placement of the sensors. These sensor locations determine the nature of the trust-set; thus it is important to locate the sensors relatively close to the expansion locations.

Yet bundled sensor locations will negatively affect the conditionality of the numerical removed model, which must share the boundary DoF locations. In equation (18) it is clearly seen that the removed model (part of the numerical parent model) is inverted in a least-squares sense. The noise characteristic of the hyrbid model is therefore affected by the conditionality of the numerical model.

It is clear that an optimum must be found between bundling the sensors near the expanded DoF locations and spreading them around the structure for a better removed model conditioning.

2.1.3 The setup

For SEMM two sets of FRFs of the same subframe are required, a parent model and an overlay model. The parent model comprises the DoF-set for the expansion and the same DoF-set as the overlay model. The parent FRF-model is obtained from a Finite Element model of the subframe of which FRFs are synthesized by mode-superposition of 500 modes, which corresponds to roughly 4.5 kHz. The overlay model provides the accurate dynamics. These FRFs are obtained by an impact test on the physical subframe. In the following, an overview of the three models used in the SEMM calculation is shown:

1. *Parent model*: The FE-based FRF model $\left(\mathbf{Y}^{\text{parent}} \in \mathbb{C}^{198\times219}\right)$. This model has the larger DoF set on which the overlay model is expanded and can be seen as the provider for the high spatial resolution in the SEMM model;

2. *Overlay model*: These FRFs provide the accurate dynamics or 'trust-set FRFs'. The subframe is instrumented with nine triaxial accelerometers, one on every coupling point and one on another (random) position. In total 48 impact locations were distributed over the structure. From this measurement set-up, a subset of measured FRFs were chosen ($\mathbf{Y}^{\text{ov}} \in \mathbb{C}^{20\times33}$);

3. *Removed model*: This subset from the parent model and makes place for the overlay model.

DoFs	**Channels**	**RefChannels**	
Measurement	20	33	
Coupling	96	96	$(8 \times 4 \times 3 = 96)$
Conditioning	75	75	
Validation	7	15	
Total	**198**	**219**	

Table 1: Overview of the SEMM measurement set-up.

Now that the sub-systems have been defined, the actual construction of the SEMM model is done according to equation (18).

As can be read in table 1, there is a set of FRFs which are *not* used in the overlay model. These measured FRFs are independent from the updated SEMM FRFs and can therefore be used for validation.

2.2 Results

In this section the results of the SEMM process are shown. In the left plot of figure 4, a subframe FRF from the FE model and a measured FRF is shown. It can be observed that even the first resonance does not match the measurement. In the right plot, a trust-set FRF (i.e. from the overlay model) is displayed. It can observed that the updated parent model follows the overlay model exactly as required by the method.

In figure 5, two SEMM FRFs are shown against a validation measurement. It can be observed that the SEMM expanded DoF adhere to the validation FRF in the low frequency regime very well. At higher frequencies, although the resonance frequencies themselves are accurate, the FRF from the SEMM model diverge from the validation measurements. At these frequencies the delta between the implicit numerical and experimental mode-shapes is too large, and the hybrid model can no longer properly match the FRF due to the inadequate numerical manifold. Nevertheless the FRF are deemed satisfactory for the virtual point method in DS.

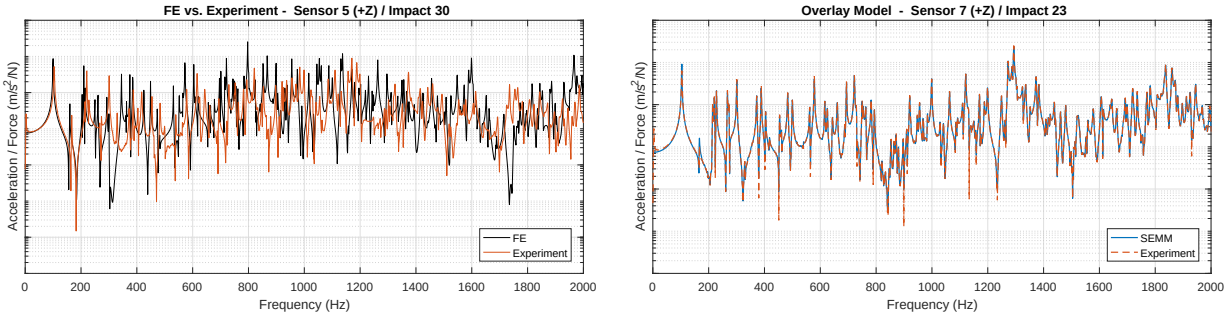

Figure 4: In the left figure a synthesized FRFs is shown against a measured FRF. In the right figure, boundary DoF SEMM FRF from the overlay model is shown. A clear 1-to-1 match to the measurement is observed as required by the method.

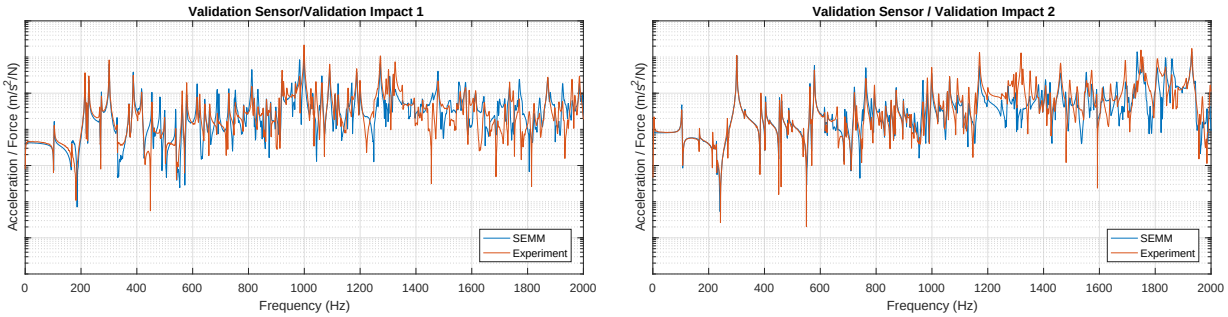

Figure 5: SEMM Results: In the left and right figures, internal validation DoF FRFs are shown; a close match is apparent at lower frequencies, yet the SEMM model diverges when the numerical parent model is no longer representative of the measured structure.

As a side-note; note the high frequency density of the subframe. It becomes apparent that expansion methods whose expansion basis is that of a limited set of numerical modes, such as SEREP and VIKING, would have a hard time capturing the number of modes present in a relatively low frequency band.

2.3 Part 2: Frequency-Based Substructuring

In section 2.1 an FRF model of the vehicle's subframe has been obtained. As mentioned, the test-based modelling of the EDU and the characterisation of the rubber decoupling mounts are not shown in this paper. The transfer dynamic stiffness rubber decoupling elements are obtained using the in-situ approach as described in [8]. This cannot be used as a subsystem in the LM-FBS equation (7), as the point stiffness is not available. Therefore, to use this transfer stiffness correctly, it is used in the weakened LM-FBS relation (11).

In figure 6 the coupling results are shown for a force excitation on the EDU to a response on the subframe validation sensor. The main tendency of the assembled FRFs shows that the global trend is captured very well, which is especially well depicted in the graphs below of the same transfer functions, shown in 12^{th} octave bands. The assembled system shows a very damped response, although the subframe does clearly not, as can be seen in the figures 5. This can be explained by the coupling to neighboring substructures which are very heavily damped.

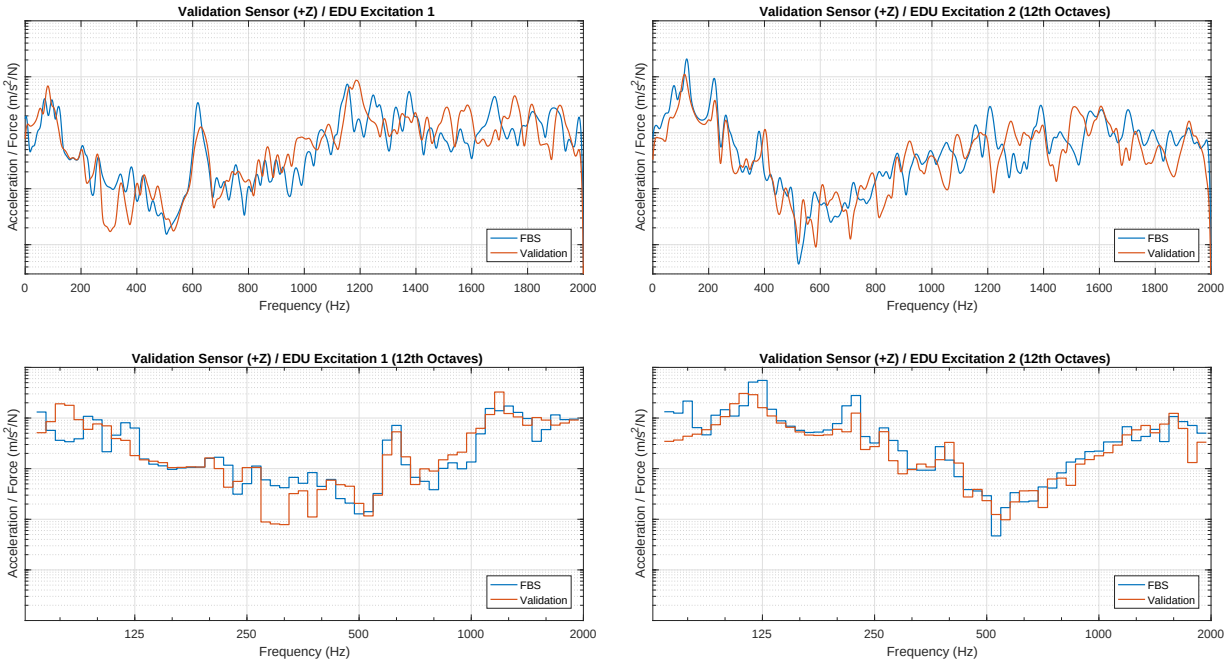

Figure 6: FBS Results compared with validation, the excitation and response locations are shown in fig. 1.

2.4 Discussion

The sensor and impact locations were chosen based on a "best guess" of the optimum in the matrix conditioning vs. interface observability problem stated in section 2.1.2. Furthermore, the number of sensor and impact channels was limited by the equipment and time available. The quality of the SEMM model is case specific; finding an optimum in resources (time or otherwise) vs. model accuracy is still largely a grey area. This holds for determining the optimum in both the number and location of sensor/impacts. More research is warranted to find an optimal resources vs. accuracy curve which will, in turn, enhance the practical applicability of SEMM.

3 Conclusions

This paper is concerned with the application of the System Equivalent Model Mixing (SEMM) method on a subframe of a hybrid vehicle. Practical considerations are stipulated on how the method is applied successfully. It is demonstrated how the obtained FRF-model of the subframe can be applied in the LM-FBS

framework along with its neighbouring substructures to construct an assembly. To establish the connectivity between all components in the translational and rotational degrees of freedom the virtual point transformation is used. It is shown that the various modelling strategies result in a full-system prediction of structural vibrations well into the kHz-range.

For future vehicle engineering, this DS assembly can be extended with noise transfer functions (NTFs) from the subframe coupling points to microphones in the cabin of the vehicle. For prediction of in-vehicle noise levels, the DS assembly can by combined with a description of the active source (EDU), such as blocked forces or free-velocities [11].

Acknowledgments

This project has been a collaboration between Volvo Car Group and VIBES.technology.

References

[1] D. Lennström, A. Nykänen, "Interior sound of today's electric cars: Tonal content, levels and frequency distribution", Technical Report 2015-01-2367, SAE Technical Paper, 2015, DOI: 10.4271/2015-01-2367.

[2] D. de Klerk, D. J. Rixen, S. N. Voormeeren, "General framework for dynamic substructuring: History, review and classifcation of techniques", *AIAA Journal*, 46(8):1169–1181, 2008, DOI: 10.2514/1.33274.

[3] E. Barten, M. V. van der Seijs, D. de Klerk, "A complex power approach to characterise joints in experimental dynamic substructuring", in: *Dynamics of Coupled Structures*, *Proceedings of the 32nd IMAC, A Conference and Exposition on Structural Dynamics*, volume 1, chapter 27, 281–296, Springer New York, 2014, DOI: 10.1007/978-3-319-04501-6_27.

[4] S. W. Klaassen, M. V. van der Seijs, D. de Klerk, "System equivalent model mixing", *Mechanical Systems & Signal Processing*, 105:90 – 112, 2018, DOI: https://doi.org/10.1016/j.ymssp.2017.12.003.

[5] M. V. van der Seijs, D. D. van den Bosch, D. J. Rixen, D. de Klerk, "An improved methodology for the virtual point transformation of measured frequency response functions in dynamic substructuring", in: M. Papadrakakis, V. Papadopoulos, V. Plevris (eds.), *4th ECCOMAS Thematic Conference on Computational Methods in Structural Dynamics and Earthquake Engineering (COMPDYN)*, 4334–4347, Kos Island, Greece, 2013, DOI: 10.7712/120113.4816.C1539.

[6] E. A. Pasma, M. V. van der Seijs, S. W. B. Klaassen, M. W. van der Kooij, "Frequency Based Substructuring with the Virtual Point Transformation, Flexible Interface Modes and the Transmission Simulator", in: *Proceedings of the XXXV International Modal Analysis Conference (IMAC), Orlando, FL*, 2018.

[7] D. de Klerk, D. Rixen, S. Voormeeren, F. Pasteuning, "Solving the RDoF problem in experimental dynamic substructuring", in: *Proceedings of the XXVI International Modal Analysis Conference (IMAC), Orlando, FL*, Society for Experimental Mechanics, Bethel, CT, 2008.

[8] J. Meggit, A. Elliot, A. Moorhouse, "In-situ determination of dynamic stiffness for resilient elements", *Journal of Mechanical Engineering Science*, 230(6):986–993, 2015.

[9] J. C. O'Callahan, P. Avitabile, R. Riemer, "System equivalent reduction expansion process (SEREP)", in: *Proceedings of the VII International Modal Analysis Conference (IMAC), Boston, MA*, volume 1, 29–37, Society for Experimental Mechanics, Bethel, CT, 1989.

[10] L. Thibault, A. Butland, P. Avitabile, "Variability improvement of key inaccurate node groups – viking", in: R. Allemang, J. De Clerck, C. Niezrecki, J. Blough (eds.), *Topics in Modal Analysis II, Volume 6*, 603–624, Springer New York, New York, NY, 2012.

[11] M. V. van der Seijs, D. de Klerk, D. J. Rixen, "General framework for transfer path analysis: History, theory and classification of techniques", *Mechanical Systems & Signal Processing*, 68–69:217–244, 2016, DOI: 10.1016/j.ymssp.2015.08.004.